

GT2011-46949 -

ROTOR DYNAMICS ANALYSIS AND TESTING OF A TURBOMOLECULAR PUMP ROTOR-BEARING SYSTEM

¹Chih-Neng Hsu, ²Hsiao-Wei D. Chiang, ²Yu-Meng Huang, ²Ying-Chia Fu, ³Kuo-Hsun Hsu, and ³Chao-Huan Li

¹Assistant Professor, Department of Refrigeration, Air Conditioning and Energy Engineering,
National Chin-Yi University of Technology, Taichung City, 41111, Taiwan, Republic of China

²Department of Power Mechanical Engineering, National Tsing Hua University,
Hsinchu City, 30013, Taiwan, Republic of China

³Prosol Corporation, Hsinchu County, 30252, Taiwan, Republic of China

ABSTRACT

This study is focused on the dynamic characteristics of a vertical turbomolecular pump (TMP) rotor-bearing system. The research methods can be divided into two parts, which are numerical analysis and experimental measurements. In numerical analysis, we use the finite element analysis software DyRoBeS and ANSYS to construct a two- and three-dimensional models of the rotor-bearing system. In the analysis process, by using the pump system assembly testing data, we can verify the rotor-bearing system finite element models under different boundary conditions. Next, we calculate the Campbell diagram to study the dynamic characteristics of the rotor-bearing system, and to compare with the experimental results to verify the models. Finally, we found the relationship between the rotor critical speed and the bearing stiffness in order to study the design of the molecular pump rotor and the bearing system. Experimental measurements were divided into two parts: static modal tests and dynamic measurements. Static modal tests can provide the natural frequencies of the rotor-bearing system. Waterfall diagrams of the dynamic tests can measure the pump system critical speed from zero speed up to the working speed crossing, and to insure that the pump working speed is far from the critical speed of at least 10% in the safe margin. In summary, the results of the experimental measurements and numerical analysis can provide the basis for the design tool for turbomolecular pump rotor-bearing system in order to identify and prevent pump vibrations.

Keywords: turbo molecular pump, rotor-bearing, mode shape, vibration characteristics, critical speed

NOMENCLATURE

DyRoBeS	Dynamics Rotor Bearing System
FEM	Finite element methods
FFT	Fast Fourier Transform
H(f)	Frequency Response Function
TMP	Turbomolecular Pump
x_1, y_1	represent node 1's displacements, and,
x_2, y_2	represent node 2's displacements
Greek Symbols	

$\{\phi\}$	The amplitude displacement vector or eigenvector and
θ_{x1}, θ_{x2}	represent node 1's displacements
θ_{x2}, θ_{y2}	represent node 2's displacements
ω_j	The natural frequency or eigenvalue

INTRODUCTION

Finite element methods (FEM) have been used in rotordynamic analyses since 1970. In the early days, only the bending vibrations under rotor linear displacement conditions were considered. Later on, rotor models were improved to include rotation inertia, gyroscopic moments, axial loads, internal and external damping, and shear deformations. Hibner [1] used a unique transfer matrix method applied to an idealized equivalent engine system for predicting vibratory responses that accounted for nonlinear viscous damping effects. Glasgow and Nelson [2] applied a common mode synthesis method and showed that a significant reduction in the scope of the problem is achieved when analyzing the stability of a dual rotor system. Li and Hamilton [3] applied a simplified transfer matrix method with squeeze film dampers on two-spool rotor systems. Huang [4] developed a transfer matrix impedance coupling method to predict frequency responses of multiple rotor systems. Zeng and Hu [5] used a gyroscopic mode synthesis technique for multishaft rotor-bearing-casing systems. Gupta *et al.* [6] used a modified transfer matrix method to study the energy distributions in a multispool rotor system. However, due to assumptions of the transfer matrix method [7], it sometimes resulted in numerical instability problems or in missing-root problems [8].

In this article, the presented analyses are based on the methods used by Nelson [9, 10] and Lalanne [11]. The finite element rotor-bearing system models were established using inertial coordinate systems. The models were used to predict natural frequencies, mode shapes, critical speed maps, and bearing stiffness. Figure 1 shows the TMP analysis system development flow chart. Based on the Lagrangian formulation, this general model of continuous rotor-bearing systems was

established and the gyroscopic moments, rotary inertias, bending, and shear deformations are included. The rotor-bearing analysis system was then applied to the turbomolecular pump system applications and can provide industry with design guidelines for future TMP developments.

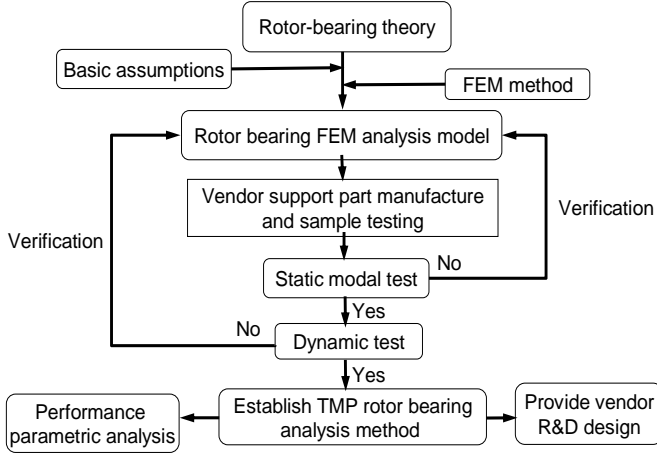


Figure 1. Molecular Pump Rotor-Bearing System Analysis Flow Chart

ROTOR-BEARING SYSTEM MODEL

Figure 2 shows a typical turbomolecular pump as will be analyzed in this study. A flexible rotor-bearing system model will be used to model the TMP and will consist of discrete disks, rotor segments with distributed masses and elastic characteristics, and discrete bearings.

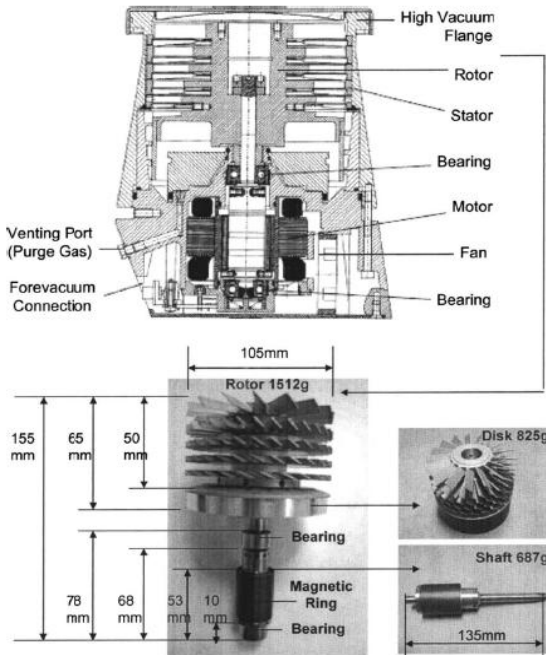


Figure 2. Parts of a Molecular Pump Dimension

A. Element Divisions and Structural Nodal Displacements

The rotor system can be divided into rigid disks, rotor segments, and linear bearing supports as shown in Figure 3. Also shown are nodal displacements in an inertial coordinate

system, where

$$\{q\} = \{x_1, y_1, \theta_{x1}, \theta_{y1}, x_2, y_2, \theta_{x2}, \theta_{y2}\}, \quad (1)$$

and where $x_1, y_1, \theta_{x1}, \theta_{y1}$ represent node 1's displacements, and $x_2, y_2, \theta_{x2}, \theta_{y2}$ represent node 2's displacements.

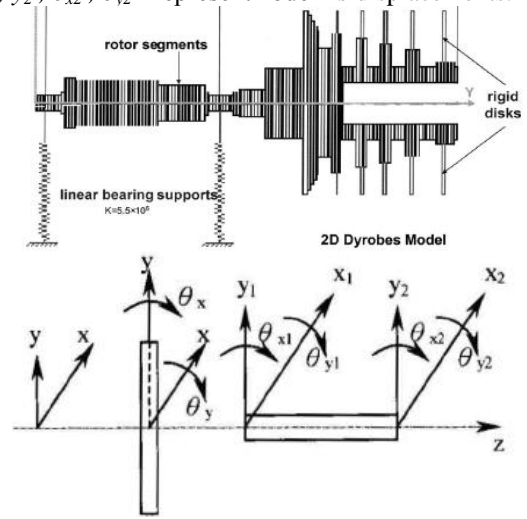


Figure 3. Rotor Element

B. Component Equations

In this section, the beam element was based on Timoshenko theory. A rigid disk equation of motion is developed for the rotor-bearing system using a Lagrangian formulation.

1. Rigid Disk

$$([\mathbf{M}_T^d] + [\mathbf{M}_R^d])\{\ddot{q}^d\} - \Omega[\mathbf{G}^d]\{\dot{q}^d\} = \{F^d\}, \quad (2)$$

where

$$[\mathbf{M}_T^d] = \begin{bmatrix} m_d & 0 & 0 & 0 \\ 0 & m_d & 0 & 0 \\ 0 & 0 & 0 & 0 \\ 0 & 0 & 0 & 0 \end{bmatrix}, \quad [\mathbf{M}_R^d] = \begin{bmatrix} 0 & 0 & 0 & 0 \\ 0 & 0 & 0 & 0 \\ 0 & 0 & I_d & 0 \\ 0 & 0 & 0 & I_d \end{bmatrix},$$

$$[\mathbf{G}^d] = \begin{bmatrix} 0 & 0 & 0 & 0 \\ 0 & 0 & 0 & 0 \\ 0 & 0 & 0 & -I_p \\ 0 & 0 & I_p & 0 \end{bmatrix}$$

2. Finite Rotor Elements

$$([\mathbf{M}_T^e] + [\mathbf{M}_R^e])\{\dot{q}^e\} - \Omega[\mathbf{G}^e]\{q^e\} + [\mathbf{K}_B^e]\{q^e\} = \{F^e\}. \quad (3)$$

In Equation (3), $[\mathbf{M}_T^e]$, $[\mathbf{M}_R^e]$, $[\mathbf{G}^e]$, and $[\mathbf{K}_B^e]$ are provided in Appendix A.

3. Linear Bearings

$$-[\mathbf{C}^b]\{\dot{q}^b\} - [\mathbf{K}^b]\{q^b\} = \{F^b\}, \quad (4)$$

where

$$[\mathbf{C}^b] = \begin{bmatrix} C_{xx} & C_{xy} & 0 & 0 \\ C_{xy} & C_{yy} & 0 & 0 \\ 0 & 0 & 0 & 0 \\ 0 & 0 & 0 & 0 \end{bmatrix}, \quad [\mathbf{K}^b] = \begin{bmatrix} K_{xx} & K_{xy} & 0 & 0 \\ K_{xy} & K_{yy} & 0 & 0 \\ 0 & 0 & 0 & 0 \\ 0 & 0 & 0 & 0 \end{bmatrix}$$

4. Rotor-Bearing System

The assembled system equation of motion, consisting of component equations of Equations (2)-(4), is of the form

$$[M]\{\ddot{q}^s\} + ([C] + \Omega[G])\{\dot{q}^s\} + [K]\{q^s\} = \{F^s\} \quad (5)$$

where $\{q^s\} = [x_l, y_l, \theta_{xl}, \theta_{yl}, \dots, x_n, y_n, \theta_{xn}, \theta_{yn}]^T$.

5. Natural Frequency Calculation

To solve for the principal mode shapes and natural frequencies of the system, we can use Equation (5) as undamped system equation of motion and without gyroscopic moments.

$$[M]\{\ddot{q}^s\} + [K]\{q^s\} = \{F^s\} \quad (6)$$

Assuming

$$\{q\} = \{\phi\}e^{i\omega_j t} \quad (7)$$

and free vibration $\{F^s\} = 0$, we have

$$([K] - \omega_j^2[M])\{\phi\} = \{0\} \quad (8)$$

For nontrivial solutions for $\{\phi\}$, we need to satisfy the following:

$$\det([K] - \omega_j^2[M]) = 0 \quad (9)$$

where $\{\phi\}$ is the amplitude displacement vector or eigenvector and ω_j is the natural frequency or eigenvalue. By solving Equation (9), we can have the natural frequency ω_j .

Then by substituting ω_j into Equation (8), we can solve for $\{\phi\}$. For system vibration at ω_j , we have the principal mode shape as

$$\{\phi^{(r)}\} = \{\phi_1^{(r)} \phi_2^{(r)} \phi_3^{(r)} \dots \phi_n^{(r)}\} \quad (10)$$

Each frequency will have its corresponding mode shape. By combining all the corresponding frequencies and mode shapes, we will have the principal mode shapes for the entire system,

$$\{\phi\} = [\{\phi^{(1)}\} \{\phi^{(2)}\} \{\phi^{(3)}\} \dots \{\phi^{(n)}\}] \quad (11)$$

6. Rotor System Critical Speed Calculation

In order to solve for the critical speed of the system, we need to solve the following homogeneous Equation (12):

$$[M^s]\{\ddot{q}^s\} + [C^s]\{\dot{q}^s\} + [K^s]\{q^s\} = \{0\} \quad (12)$$

In other words, it is an eigenvalue problem. In structural dynamics, there are many ways to solve a large-scale sparse matrix eigenvalue problem. However, it is only good for small damping and symmetrical matrices. Since we have included the effects of gyroscopic moments, anisotropic bearings, and material damping, the damping and stiffness matrices become nonsymmetric and dependent on speed. Therefore, we have to solve the Equation (12) in a different way. Normally we may reduce the second order homogeneous Equation (12) into $2n$ times first order differential equations. Introducing the $2n$ order column vector $\{x\}$,

$$\{X\} = \begin{Bmatrix} \dot{q} \\ q \end{Bmatrix} \quad (13)$$

Equation (12) can be expressed as

$$\begin{bmatrix} \underline{0} & M \\ M & C \end{bmatrix} \begin{Bmatrix} \dot{q} \\ q \end{Bmatrix} + \begin{bmatrix} -M & \underline{0} \\ \underline{0} & K \end{bmatrix} \begin{Bmatrix} \dot{q} \\ q \end{Bmatrix} = \begin{Bmatrix} \underline{0} \\ \underline{0} \end{Bmatrix} \quad (14)$$

Equation (14) can be simplified as Equation (15),

$$[A]\{\dot{X}\} + [B]\{X\} = \{0\} \quad (15)$$

Now assuming

$$\{x\} = \{\phi\}e^{\lambda t} \quad \text{and} \quad \{\dot{x}\} = \lambda\{\phi\}e^{\lambda t} \quad (16)$$

Substituting Equation (16) into Equation (15), we have

$$(\lambda A + B)\{\phi\} = 0 \quad (17)$$

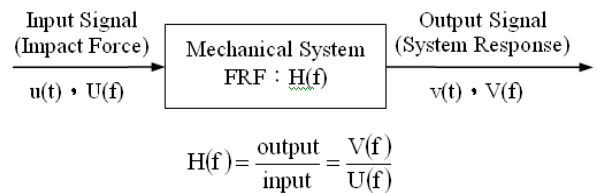
Using QR or Lanczos method, we can solve for the eigenvalues and eigenvectors for Equation (17). Due to Equation (14) containing the damping term C, the eigenvalues and eigenvectors are complex numbers. From the eigenvalue $\lambda_K = \alpha_K \pm i\omega_K$, we can find out the damped critical speed and the onset of speed instability.

RESULTS AND DISCUSSION

Static and dynamic testing was performed to investigate the TMP rotor-bearing system. Three static tests were performed including (1) rotor shaft only static testing, (2) pump rotor static testing, and (3) pump assembly static testing. Finally, dynamic testing was performed.

Rotor Shaft Only Static Testing (1)

In this study, a hammer impact experimental method is used. A free-free support boundary condition was assumed for the modal testing, which implies that the test object is unconstrained. In order to satisfy this assumption, the test object was suspended using an elastic string to simulate the free support condition. An impact hammer was then used with a load cell to apply the impact force. An accelerometer on the test object recorded the response due to the impact. Both the impact force and the response are amplified and input to a Fast Fourier Transform (FFT) analyzer to obtain a Frequency Response Function (H(f)). Through the use of a routine identification procedure, the mode shape related parameters could be determined. An experimental setup is shown in Figure 4.



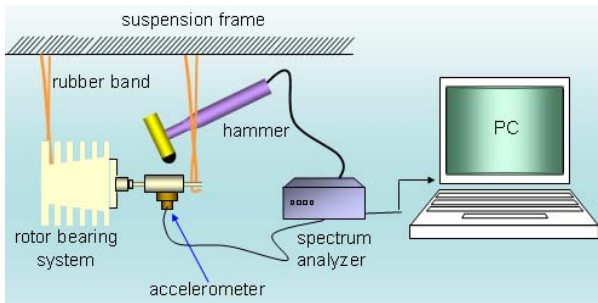


Figure 4. Single Input and Output System and Free-Free Modal Testing Facility

For the rotor shaft only static test (rotor shaft as shown in Figures 8&9), the first two mode frequencies were found as following: F1 is 2,191 Hz, and F2 is 9,000 Hz, as shown in Figure 5.

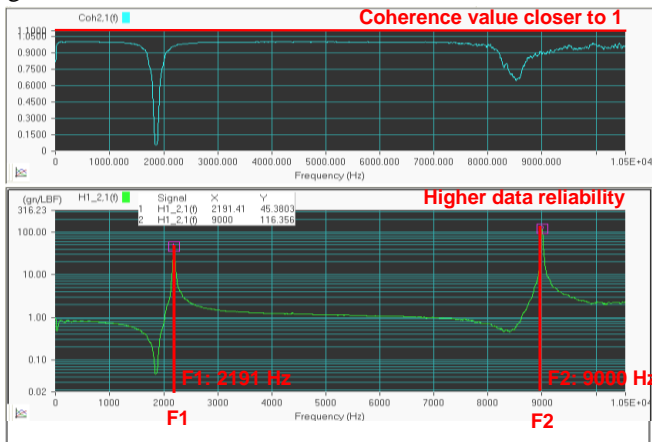


Figure 5. Shaft Frequency Response Function

Pump Rotor Static Testing (2)

After we assembled the entire rotor including the shaft and rotor blades (as shown in Figures 10&11) and performed the static test, the first six mode frequencies (1 from rotor shaft and 5 from rotor blades) were found as shown in Table 1.

Table 1. Rotor Static Free-Free Modal Testing

Frequency	F1 (Rotor)	F1 (Blade)	F2 (Blade)	F3 (Blade)	F4 (Blade)	F5 (Blade)
Hz	1,125	1,599	2,115	2,630	3,375	5,296

Pump Assembly Static Testing (3)

In order to test the complete pump assembly, we further assembled the entire pump including the shaft, the rotor blades, the stator vanes, the casing, and all the rest to complete the pump module and to perform the static test. As shown in Table 2, we found two frequencies: F1 is 100 Hz, and F2 is 1,200 Hz.

Table 2. Rotor Assembly Static Modal Testing

Frequency	F1	F2
Hz	100	1,200

It was interesting to find the lower 100 Hz frequency, which was not present from the previous component static test. We concluded this low frequency is from the complete assembly of the TMP, as shown in Figure 2.

Dynamic Testing (4)

Figure 6 shows a molecular pump dynamic testing facility established for this study. This facility was composed of the turbomolecular pump, a test stand, instrumentation, and a PC based data acquisition system. An accelerometer was mounted on the pump to measure the critical speeds.

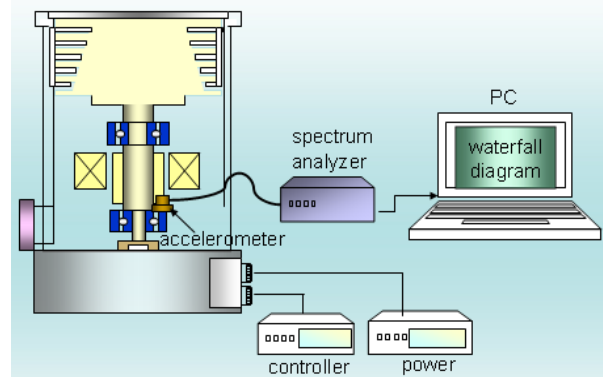


Figure 6. Molecular Pump Dynamic Testing Facility

Figure 7 shows the order tracking plot results from the engine dynamic testing. The 1st order and the 2nd order critical speed were 117Hz and 492Hz as obtained from the test results shown in Figure 7. Comparing the later calculated critical speed map results (Figure 13) with the results from dynamic testing, both the front and the rear bearing stiffness can be roughly estimated to be 5.0×10^5 N/m.

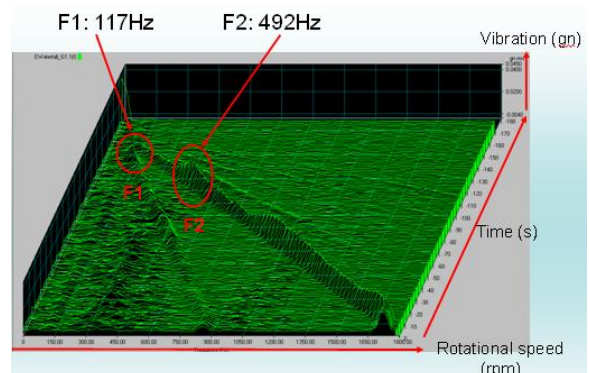


Figure 7. Molecular Pump Dynamic Testing Waterfall

FINITE ELEMENT MODEL RESULTS

Using equation (5), the first six (6) mode frequencies and mode shapes were solved using two analyses, DyRoBeS and ANSYS, producing the results shown in Figures 8-11. DyRoBeS is considered a 2D analysis tool for rotor dynamics, while the ANSYS code is a full 3D simulation model. For the rotor shaft only static test (1), Figures 8 and 9 show the first and the second mode shapes predicted by both DyRoBeS and

ANSYS. Table 3 has demonstrated that both DyRoBeS and ANSYS agree well with the test data (within 2% error).

Table 3. Shaft Static Free-Free Modal Testing and Simulation

Item	F1(Hz)	F2(Hz)
Testing	2,191	9,000
DyRoBeS	2,210	9,149
Error	1.0%	1.6%
ANSYS	2,160	9,013
Error	1.5 %	0.1%

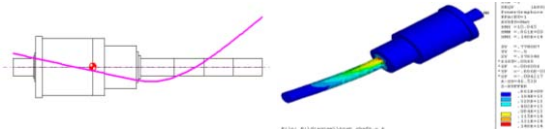


Figure 8. Shaft in the 1st Mode Shape (Free-Free Simulation)

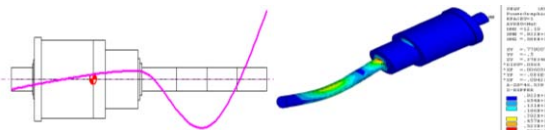


Figure 9. Shaft in the 2nd Mode Shape (Free-Free Simulation)

Table 4 was for the pump rotor static test (2) comparison. Figure 10 shows the first mode shape predicted by both DyRoBeS and ANSYS. As DyRoBeS model shows, the first mode frequency is from the shaft first bending mode. The ANSYS model showed similar results for the rotor shaft first mode. Table 4 shows both code predictions agree well with the data. In addition, Table 5 ANSYS results are showing the 2nd-6th mode frequencies are from the first bending mode of the 1st-5th stage rotor blades with good agreements with the data. This is beyond DyRoBeS code can predict since these are blade modes.

Table 4. Rotor Static Free-Free Modal Testing and Simulation

Item	F1(Hz)
Testing	1,125
DyRoBeS	1,165
Error	3.4%
ANSYS	1,087
Error	3.4%

Table 5. Blade Static Modal Testing and Simulation

Item	L1	L2	L3	L4	L5
Testing	1,599	2,115	2,630	3,375	5,296
ANSYS	1,532	2,068	2,670	3,354	5,035
Error	4.2%	2.2%	1.5%	0.6%	5.0%

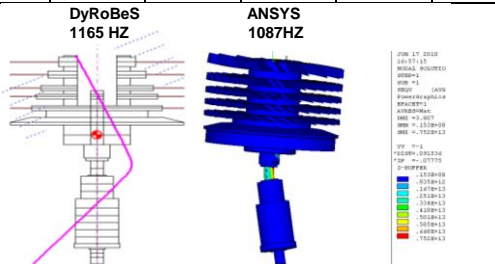


Figure 10. Rotor in the 1st Mode Shape (Free-Free Simulation)

For the pump assembly static test (3), Figure 11 has predicted the first 3 mode shapes for the assembled pump static test by both DyRoBeS and ANSYS. Table 6 shows the comparison with the data. As shown, the first and third mode frequencies from both codes agree well with the data, except that the second mode frequency was not found from the test data. However, later during the dynamic test (4), we were able to confirm the existence of the second mode.

Table 6. Rotor Assembly Modal Testing and Simulation

Item	F1	F2	F3
Testing	100	N/A	1,200
DyRoBeS	96	381	1,222
Error	4.0%	N/A	1.8%
ANSYS	102	435	1,160
Error	2.0%	N/A	3.3%

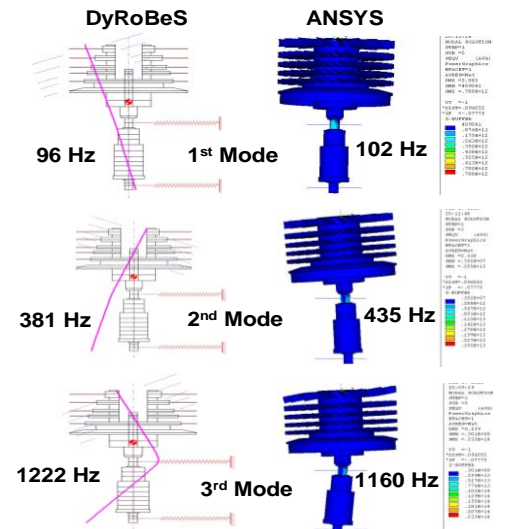


Figure 11. Rotor Assembly in the 1st, 2nd, and 3rd Mode Shape

For the dynamic test (4), only ANSYS was used for the predictions since DyRoBeS neglects the centrifugal effects. Table 7 shows very good agreement between the data and the analysis. Also, the missing 400 Hz frequency from the static test was verified from both the data and the analysis.

Table 7. Rotor Critical Speed Testing and Simulation

Item	F1	F1
Testing	117	492
ANSYS	111 (Forward)	520 (Forward)
Error	5.1%	5.4%

Figure 12 was created using ANSYS to predict the TMP's Campbell diagram. The Campbell diagram predicted the first and second crossings will be at 6,600 rpm and 31,000 rpm,

respectively. However, the third crossing will be well above the operating point of 51,600 rpm. Therefore, we can conclude that the TMP will have enough safety margins for the operating point. From the foregoing, it is concluded that the analyses correlate reasonably well with all the test data.

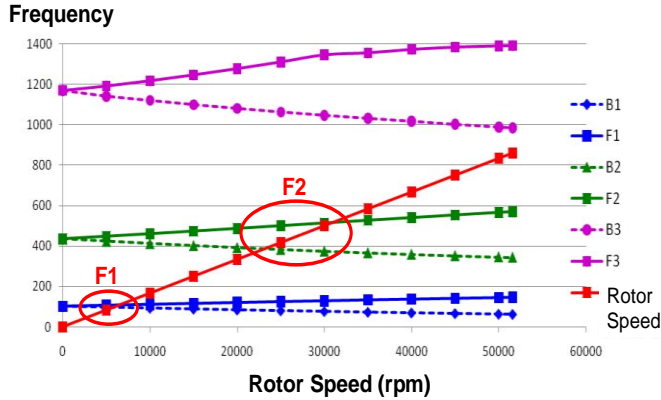


Figure 12. Rotor-Bearing System Campbell Diagram

CRITICAL SPEED MAP CALCULATION

By neglecting the damping term in Equation (5), and transferring to rotating coordinate system or rotor symmetry condition, we can obtain the critical speed map directly as shown in Figure 13. This map is based on the assumptions of equal stiffness for both front and rear bearings. Comparing the critical speed map results with results from dynamic testing, we can roughly estimate both the front and rear bearing stiffness to be 5.0×10^5 N/m. Therefore, the pump operation close to the critical speeds should be avoided to prevent bearing damage. If the pump rotor support design could be modified to a stiffer support ($K > 5.0 \times 10^5$ N/m), then a comfortable speed margin could be maintained between the operating speed (51,600 rpm) and the second order critical speed. Also shown in Figure 13, the rotor-bearing system with elastic supports has first and second critical speeds that increase as the stiffness increase, while the third order critical speed is almost constant. However, with a rigid support condition, the first two critical speeds remain almost constant as the stiffness is increased, while the third critical speed increases with the increase in the stiffness due to gyroscopic effects.

The first three critical speed mode shapes were also shown in Figure 11. The second order critical speed mode shape seems most likely to cause the frequent damages of the pump bearing near the bottom end.

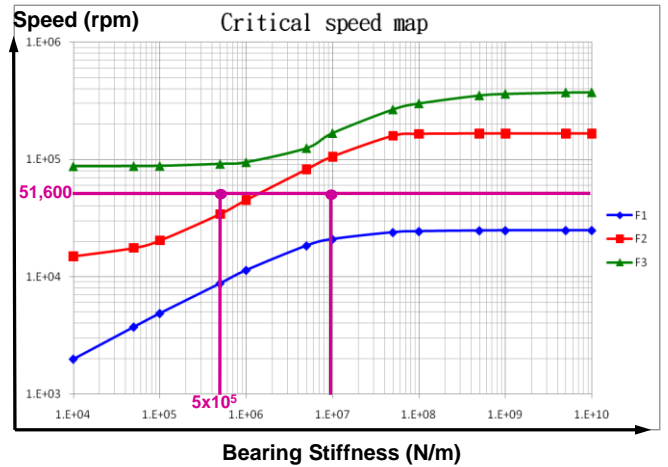


Figure 13. Rotor System Critical Speed Map

CONCLUSIONS

In this study, we are using a typical small size turbomolecular pump as our test study. Two finite element model analyses, DyRoBeS and ANSYS, were used to predict the natural frequencies and mode shapes, to produce Campbell diagrams and critical speed maps, and to estimate the bearing stiffness. Both theoretical and experimental analyses were used to study the rotor-bearing system. Modal testing and dynamic test were used to verify the analytical results, including the Campbell diagrams, critical speed maps and the bearing stiffness.

Using 2D DyRoBeS model, very good results can be obtained for the rotor shaft frequencies and mode shapes. However, the full 3D ANSYS model does provide more detailed analysis for the complete rotor blade model as well as the dynamic test simulations. Very good agreement was demonstrated between the overall analyses and the test data. The analysis demonstrated that the rotor operation of 51,600 rpm is very close to the 2nd critical speed, which may have caused the recent pump bearing failures near the pump bottom. The analysis can also provide guidelines to avoid the second order critical speed mode shape failures.

ACKNOWLEDGMENTS

The authors would like to thank the National Science Council (NSC) and MOEA SBIR project, for their support for the SOFC/GT/CCHP Investigation Program (NSC 99-2622-E-007-008-CC3, SBIR: 1Z980782)

REFERENCES

1. D. H. Hibner, "Dynamic Response of Viscous-damped Multi-shaft Jet Engines," *Journal of Aircraft*, Vol. 12, No. 4, pp. 305–312, 1975.
2. D. A. Glasgow and H. D. Nelson, "Stability Analysis of Rotor Bearing Systems Using Component Mode Synthesis," *The American Society of Mechanical Engineers*, New York, 1979.
3. Q. Li and J. F. Hamilton, "Investigation of the Transient

- Response of a Dual-Rotor System With Intershaft Squeeze Film Damper,"ASME Journal of Engineering for Gas Turbines and Power, Vol.108, pp.613-617, 1986.
4. T. Huang, "Modal Testing and Analysis," The American Society of Mechanical Engineers, New York, pp. 71-76, 1987.
 5. Z. C. Zheng and Y. Hu, "Vibration in Rotating Machinery," Institution of Mechanical Engineers Conference Publication, Paper No. C245/88, pp. 607-614, 1988.
 6. K. D. Gupta, K. Gupta, and K. Athre, "Stability Analysis of a Dual Rotor System by Extended Transfer Matrix Method," The 34th ASME Proceedings of ASME TURBO EXPO 1989: Land, Sea, and Air, The American Society of Mechanical Engineers, International Gas Turbine Institute, Toronto, Paper 89-GT-194, 1989.
 7. Y. Kazao and E. J. Gunter, "Dynamics of Multi-Spool Gas Turbines Using The Matrix Transfer Method-Theory," International Journal of Turbo and Jet Engines, Vol. 06, pp.153-161, 1989.
 8. A. Peduzzi, "Simulation of Advanced Engine Lubrication and Rotor Dynamics Systems Rig Design and Fabrication," AIAA Paper No.83-1133, 1983.
 9. H. D. Nelson and J. M. McVaugh, "The Dynamics of Rotor-Bearing Systems Using Finite Elements," ASME Journal of Engineering for Industry, Vol. 98, pp. 593-600, May 1976.
 10. H. D. Nelson, "A Finite Rotating Shaft Element Using Timoshenko Beam Theory," ASME Journal of Mechanical Design, Vol. 102, pp. 793-803, 1980.
 11. M. Lalanne and G. Ferraris, Rotordynamics Prediction in Engineering, Wiley, New York, pp. 86-88, 1990.
 12. R. L. Ruhl and J. F. Booker, "A Finite Element Model for Distributed Parameter Turbo Rotor Systems," ASME Journal of Engineering for Industry, Vol. 94, pp. 126-132, 1972.
 13. Hsiao-Wei D. Chiang and Chih-Neng Hsu, "A Microturbine Rotor-Bearing System Analysis," ASME IGTI TURBO EXPO, GT-2002-30316, Amsterdam, Netherlands, June 2002.
 14. Hsiao-Wei D. Chiang, C. P. Kuan, and H. L. Li, "Turbo Molecular Pump Rotor-Bearing System Analysis and Testing," Journal of American Vacuum Society, Vol.27, No.05, pp.1196-1203, 2009.
 15. Erik Swanson, Chris D. Powell, and Sorin Weissman, "A Practical Review of Rotating Machinery Critical Speeds and Modes," Journal of Sound and Vibration, Vol. 08, pp.10-17, May 2005.

